The primary and three-dimensional structures of a nine-haem cytochrome *c* from *Desulfovibrio desulfuricans* ATCC 27774 reveal a new member of the Hmc family

Pedro M Matias[1], Ricardo Coelho[1], Inês AC Pereira[1], Ana V Coelho[1,2], Andrew W Thompson[3], Larry C Sieker[1,4], Jean Le Gall[1,5] and Maria Arménia Carrondo[1]*

Background: Haem-containing proteins are directly involved in electron transfer as well as in enzymatic functions. The nine-haem cytochrome *c* (9Hcc), previously described as having 12 haem groups, was isolated from cells of *Desulfovibrio desulfuricans* ATCC 27774, grown under both nitrate- and sulphate-respiring conditions.

Results: Models for the primary and three-dimensional structures of this cytochrome, containing 292 amino acid residues and nine haem groups, were derived using the multiple wavelength anomalous dispersion phasing method and refined using 1.8 Å diffraction data to an R value of 17.0%. The nine haem groups are arranged into two tetrahaem clusters, with Fe–Fe distances and local protein fold similar to tetrahaem cytochromes c_3, while the extra haem is located asymmetrically between the two clusters.

Conclusions: This is the first known three-dimensional structure in which multiple copies of a tetrahaem cytochrome c_3-like fold are present in the same polypeptide chain. Sequence homology was found between this cytochrome and the C-terminal region (residues 229–514) of the high molecular weight cytochrome *c* from *Desulfovibrio vulgaris* Hildenborough (*Dv*H Hmc). A new haem arrangement in domains III and IV of *Dv*H Hmc is proposed. Kinetic experiments showed that 9Hcc can be reduced by the [NiFe] hydrogenase from *D. desulfuricans* ATCC 27774, but that this reduction is faster in the presence of tetrahaem cytochrome c_3. As Hmc has never been found in *D. desulfuricans* ATCC 27774, we propose that 9Hcc replaces it in this organism and is therefore probably involved in electron transfer across the membrane.

Addresses: [1]Instituto de Tecnologia Química e Biológica, Universidade Nova de Lisboa, 2780 OEIRAS, Portugal, [2]Universidade de Évora, 7000 ÉVORA, Portugal, [3]EMBL Grenoble Outstation, c/o ILL 20, BP 156, F-38042 Grenoble Cedex France, [4]Department of Biological Structure, University of Washington, Seattle, WA 98195, USA and [5]Department of Biochemistry and Molecular Biology, University of Georgia, Athens, GA 30602, USA.

*Corresponding author.
E-mail: carrondo@itqb.unl.pt

Key words: electron transfer, hydrogen metabolism, MAD phasing method, multihaem cytochrome *c*, sulphate-reducing bacteria, three-dimensional structure

Received: **5 October 1998**
Revisions requested: **4 November 1998**
Revisions received: **13 November 1998**
Accepted: **2 December 1998**

Published: **25 January 1999**

Structure 15 February 1999, **7**:119–130
http://biomednet.com/elecref/0969212600700119

Introduction

A large variety of haem-containing proteins have been isolated from sulphate-reducing bacteria (SRB) which include cytochromes directly involved in electron transfer as well as other haem-containing molecules with enzymatic functions [1]. Most cytochromes *c* found in SRB are multihaemic, the best characterised being the tetrahaem cytochrome c_3, which forms a specific interaction with hydrogenase [2] and as such is the centre of the energy metabolism in these organisms. When coupled to the oxidation of molecular hydrogen, catalysed by hydrogenase, it is capable of transferring two electrons and two protons in a concerted step through a mechanism described as a 'proton thruster' [3,4]. The nine-haem cytochrome *c* (9Hcc) was isolated from cells of the sulphate- and nitrate-reducing bacterium *Desulfovibrio desulfuricans* ATCC 27774 (*Dd* 27774). Very similar amounts of the protein were obtained from cells grown either in sulphate- or nitrate-respiring conditions, indicating that this cytochrome is constitutively synthesised under both growing conditions and hence very likely an important electron carrier in both systems [5].

This cytochrome is a monomer with a molecular mass of 37,768 kDa, determined by electrospray mass spectrometry [6]. Its first 39 amino acids were sequenced and a motif was found between amino acids 32 and 37 that seems to exist in all the presently sequenced cytochromes of the c_3 type from sulphate-reducing bacteria. The midpoint redox potentials of this cytochrome were estimated to be –69 mV, –120 mV, –248 mV and –310 mV and electron paramagnetic resonance (EPR) spectroscopy of the oxidised cytochrome shows several low-spin components with a g_{max} spreading from 3.254 to 2.983 [6]. The early finding of 12 haems in this molecule is most probably due to the uncertainties inherent to the pyridine haemochrome method of determination that was used [5]. This

method is based on the assumption that the haems should have the same extinction coefficients as the one determined for monohaem cytochrome *c* [7].

Herein we present a report of the determination of the primary and three-dimensional structures of this cytochrome using the multiple wavelength anomalous dispersion (MAD) [8] phasing method and its refinement using 1.8 Å diffraction data. The structure comprises two domains with a fold comparable to that of tetrahaem cytochromes c_3 from *Desulfovibrio spp.* and similar organisms. Comparison of the amino acid sequence of 9Hcc with the C-terminal region (residues 229–514) of the 16-haem high molecular weight cytochrome (Hmc) from *Desulfovibrio vulgaris* Hildenborough (*Dv*H) revealed striking similarities that have prompted us to propose the inclusion of 9Hcc in the Hmc family of proteins.

Results and discussion

This paper describes a well-refined model for the three-dimensional model of 9Hcc where, due to the lack of complete sequence information, most of the residues were identified by inspection of 1.8 Å electron-density maps. The proposed amino acid sequence for this cytochrome is shown in Figure 1 along with the haem-binding regions.

Model description

The Cα trace of the three-dimensional structure of 9Hcc and its haem numbering scheme are represented in Figure 2. The haem groups are numbered according to their order of bonding to the polypeptide chain through a cysteine. The model contains 292 residues plus nine haem groups. There are two molecules in the asymmetric unit, related by a noncrystallographic twofold rotation axis approximately perpendicular to the crystallographic twofold axis. There is, however, no structural evidence that the molecule should be functional as a dimer. This model corresponds to a molecular mass of 36,811 Da, consistent with the experimentally observed value of 37,768 Da [6]. It is likely that the difference will be mainly due to the eight residues that could not be identified from the electron-density maps. The unambiguous polarity of the many α helices located in the structure combined with the chain tracing restrictions imposed by the presence of nine haem groups (in all known tetrahaem cytochrome c_3 structures the protein chain first links to the haem CAB atom and then to the CAC atom) allow us to attribute a very high degree of confidence to this model. This cytochrome had been previously characterised as having 12 haem groups [5] and it was therefore a surprising result from the X-ray structure determination that only nine haem groups were found. There is, however, no question that we are dealing with the same protein: the molecular weight is very similar to that determined by electrospray mass spectrometry, the N terminus is identical and, aside from small changes due to freezing, the crystal cell parameters are the same as previously reported [6] (see Materials and methods section). As is the case in many other cytochrome *c* molecules, the polypeptide chain is wrapped around the haem groups, which are covalently attached to the chain by thioether cysteinyl bridges. Also, all haem-binding motifs are of the type C-X-X-C-H and all haem axial ligands are histidine residues. The secondary structure of both independent molecules in the crystal structure is the same, and was analysed with PROCHECK [9] according to the Kabsch and Sander algorithm [10]. The results are included in Figure 1. The 9Hcc molecule is constituted by two domains connected by a polypeptide segment, as discussed below. The first domain is designated as the N-terminal domain and the second as the C-terminal domain.

Critique of the amino acid assignment procedure

When determining an amino acid sequence from good quality high-resolution electron-density maps, the shape of their electron density can unambiguously identify many residues. This is the case with lysine, arginine, alanine, glycine, histidine, phenylalanine, tyrosine, tryptophan, proline, serine and isoleucine. Aside from the absence of hydrogen bonds, leucine can be distinguished from aspartic acid and asparagine at 1.8 Å resolution as this resolution is just sufficient to resolve the pyramidalization of the Cγ atom of leucine, in contrast with the planarity of the amide and carboxyl groups in asparagine and aspartic acid respectively. Valine and threonine can be distinguished because the latter will invariably form hydrogen bonds with other atoms in the polypeptide chain or the ordered solvent layer. However, asparagine cannot usually be distinguished from aspartic acid and likewise for glutamine and glutamic acid: not only is the overall shape of these residues similar, but also both oxygen and nitrogen terminal atoms may accept or donate hydrogen bonds. At near physiological pH values, it is rather likely that the oxygen atoms will be unprotonated and thus will act as acceptors only, whereas the nitrogen atoms will retain their protons and will act as donors. As the hydrogen atoms cannot be located in protein electron-density maps at 1.8 Å resolution, the only situation when it is possible to clearly distinguish between asparagine and aspartic acid (or glutamine and glutamic acid) is when one of the terminal atoms in these residues interacts with a mainchain carbonyl atom or one of the propionate chains in a haem group. This atom then must be nitrogen, which consequently defines the amino acid as asparagine or glutamine. All asparagine and glutamine residues in Figure 1 beyond residue 39 were identified in this way. In the case of 9Hcc, the existence of two independent molecules allows a useful cross-check since it may happen that, in the case of disorder after Cβ or Cγ, one residue will be more ordered in one chain than in the other. A case in point is given by Lys21, which is well ordered in molecule A but disordered beyond Cβ in molecule B.

Figure 1

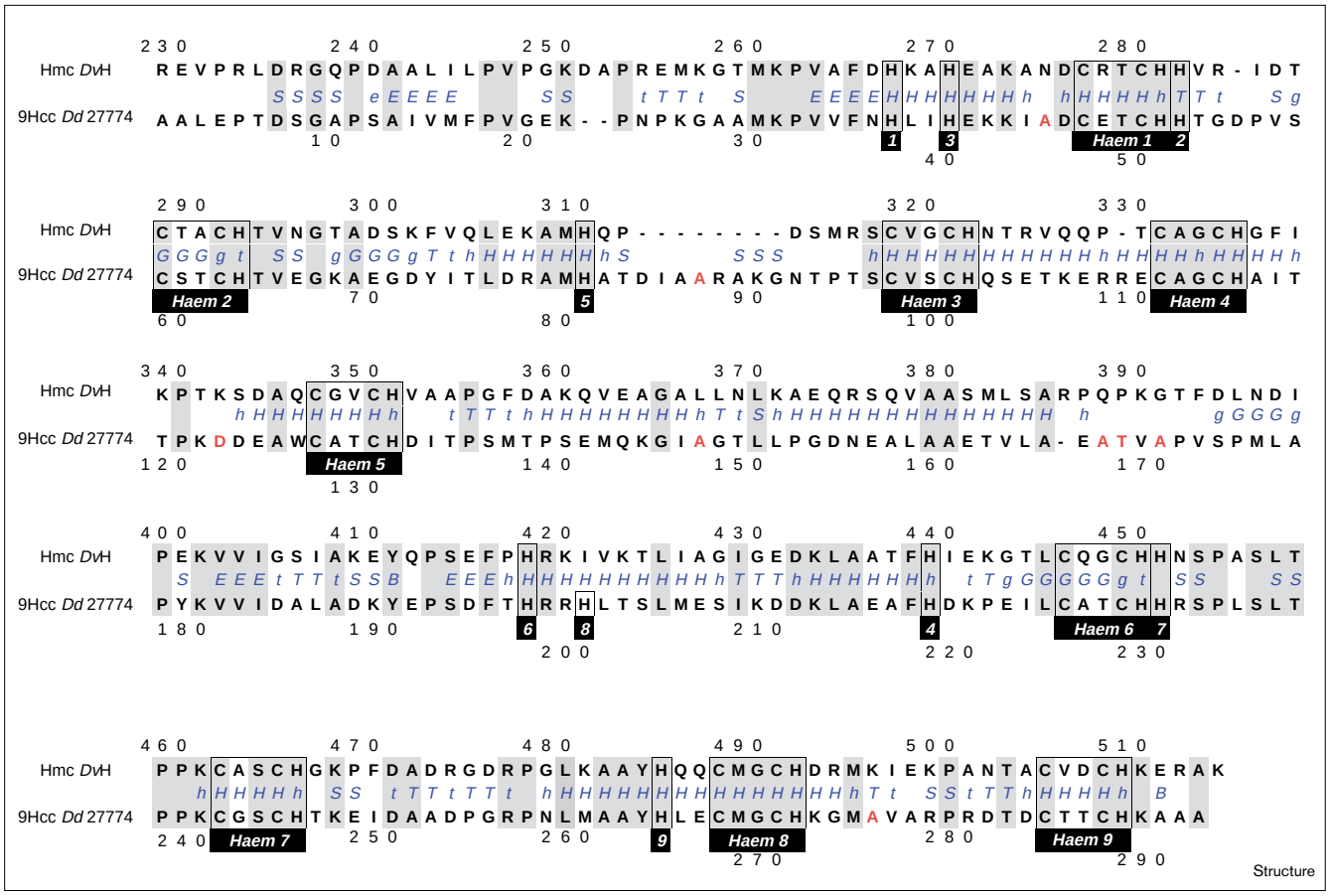

Amino acid sequence, haem-binding regions and secondary structure assignment for the nine-haem cytochrome *c* from *D. desulfuricans* ATCC 27774 (9Hcc), aligned with the C-terminal region of 16-haem high molecular weight cytochrome (Hmc) from *D. vulgaris* Hildenborough. The residue number applies to the residue directly above or below the 0 digit. The boxed residues in both Hmc and 9Hcc denote the haem-binding regions as well as the second axial ligand (histidine) of the haem Fe atoms. The identical residues between Hmc and 9Hcc are marked by shaded grey boxes. The 9Hcc residues in red are those that could not be confidently assigned from the 1.8 Å electron-density maps. Secondary structure symbols in blue, according to extended Kabsch and Sander notation, refer to 9Hcc: *B*, residue in isolated β bridge; *E*, strand in β sheet; *G*, 3_{10} helix; *H*, α helix; *S*, bend; *T*, hydrogen-bonded turn; *e*, extension of β strand; *g*, extension of 3_{10} helix; *h*, extension of α helix; *t*, extension of hydrogen-bonded turn.

Haem group geometry and environment

The nine haem groups are arranged into two tetrahaem clusters, located at both ends of the molecule, with Fe–Fe distances typical of cytochromes c_3. The extra haem is located asymmetrically between the two clusters. The first cluster is included in the N-terminal domain and the second cluster in the C-terminal domain of the 9Hcc molecule. An additional interesting feature of this structure is that this isolated haem group (haem 4) is intercalated between the haem groups (1, 2, 3 and 5) that comprise the first (N-terminal) tetrahaem cluster. This isolated haem is closest to only one haem of the N-terminal tetrahaem cluster (haem 3, 13.4 Å), but it has relatively similar Fe–Fe distances to three haem groups in the C-terminal tetrahaem cluster (haem 6, 16.2 Å; haem 7, 17.9 Å; and haem 8, 16.8 Å). The Fe–Fe distances in these tetrahaem clusters are listed in Table 1 and compared with those of tetrahaem cytochrome c_3 from the same organism [11]. The relative solvent accessibilities of the haem groups in 9Hcc were calculated with X-PLOR as previously described [11] using the Lee and Richards algorithm [12] and an H_2O probe radius of 1.6 Å. These results are also included in Table 1 and although a detailed discussion of the differences with the corresponding values for the tetrahaem cytochrome c_3 is beyond the scope of this article, the large decrease observed for haem groups 1 in 9Hcc-C and 3 in 9Hcc-N stems from the fact that these are closest to the isolated haem as discussed above and become more buried. The large increase observed in 9Hcc-C haem group 3 between molecules A and B is due not only to the slight upward motion (away from the haem) of a polypeptide segment containing Arg278, which is located at the surface

Figure 2

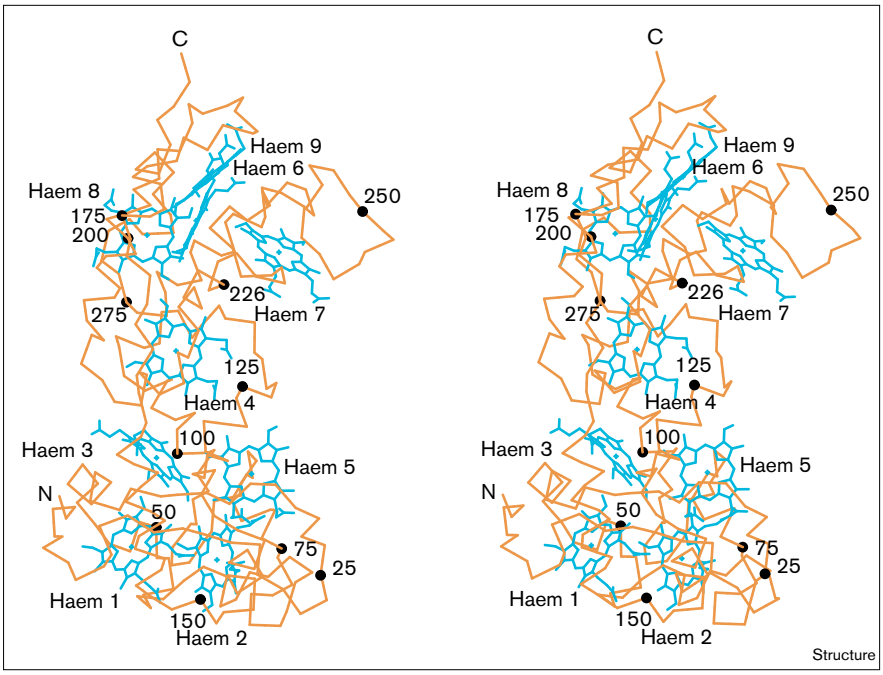

Stereoview Cα trace and haem group numbering for the three-dimensional structure of nine-haem cytochrome *c* from *D. desulfuricans* ATCC 27774. The backbone atoms are shown in orange and haems are represented in cyan. The figures were drawn with MOLSCRIPT [14].

of the molecule (Cα is shifted by 0.8 Å), but also by a radical conformational change in the sidechain of this residue: whereas in molecule A it wraps across the haem plane, in molecule B it points straight up and away from the haem group. This latter change can be attributed to different intermolecular contacts and hydrogen-bonding

Table 1

Fe–Fe distances and relative solvent exposure of the haem groups in 9Hcc and the tetrahaem cytochrome c_3 from *Dd* 27774.

		Haem 2 Fe–Fe (Å)	Haem 3 Fe–Fe (Å)	Haem 4 Fe–Fe (Å)	RSE (%)
Haem 1	c_3	12.5	11.2	17.8	10.9
	9Hcc-N	12.4 (12.6)	11.4 (11.4)	17.6 (17.8)	14.5 (15.7)
	9Hcc-C	12.5 (12.4)	12.0 (12.1)	17.5 (17.4)	8.6 (8.5)
Haem 2	c_3	–	16.3	16.8	13.1
	9Hcc-N	–	16.0 (16.0)	15.3 (15.3)	13.4 (15.1)
	9Hcc-C	–	16.8 (16.8)	16.2 (16.0)	21.4 (20.9)
Haem 3	c_3		–	12.3	18.0
	9Hcc-N		–	12.4 (12.3)	2.6 (2.5)
	9Hcc-C		–	12.2 (12.2)	10.6 (15.1)
Haem 4	c_3			–	12.8
	9Hcc-N			–	13.6 (14.1)
	9Hcc-C			–	10.5 (10.5)

Haem groups in the 9Hcc-N tetrahaem c_3-like cluster are 1,2,3,5 and in the 9Hcc-C tetrahaem c_3-like cluster are 6,7,8,9. These haem groups correspond to haems 1,2,3,4 in the tetrahaem cytochrome c_3, which is used a s reference in the table. c_3, tetrahaem cytochrome *c* from *Dd* 27774; 9Hcc-N, c_3-like tetrahaem region in the N-terminal domain of *Dd* 27774 9Hcc; 9Hcc-C, c_3-like tetrahaem region in the C-terminal domain of *Dd* 27774 9Hcc. RSE, the percentage relative solvent exposure of the haem groups. For 9Hcc, the first value in each entry refers to molecule A and the value in parentheses to molecule B; values for *Dd* 27774 c_3 were taken from [11].

Figure 3

Stereoview superposition of the nine-haem cytochrome *c* from *D. desulfuricans* ATCC 27774 c_3-like tetrahaem regions in molecule A (Cα trace shown in red, haem groups shown in yellow) and the tetrahaem cytochrome c_3 structure (107 amino acids, shown in cyan) from the same organism. The top part of the figure shows the c_3 structure superimposed onto the N-terminal tetrahaem c_3-like region. The lower part of the figure shows the c_3 structure superimposed onto the C-terminal tetrahaem c_3-like region.

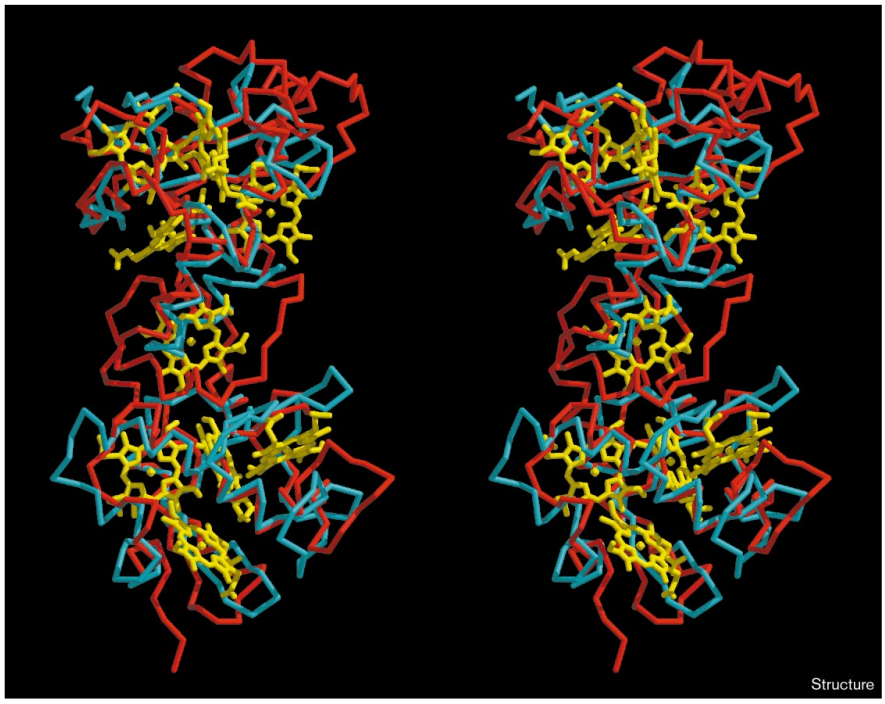

patterns. The isolated haem is nearly completely buried, with a relative solvent exposure of 0.6% for both molecules A and B. This, combined with its location in the structure, suggests that it may be connected with electron transfer between the two tetrahaem clusters.

Comparison with tetrahaem cytochrome c_3

Using the Fe atoms in each tetrahaem cluster as initial reference, both the N-terminal and C-terminal domains in the structural model of 9Hcc (molecule A) were superimposed with the known structure of tetrahaem cytochrome c_3 from the same organism [11] using TURBO [13]. All Cα atoms less than 1.5 Å apart were used in the final least-squares fit (54 for the superimposition of c_3 and 9Hcc-N; 35 for the superimposition c_3 and 9Hcc-C). The results are illustrated in Figure 3 as a MOLSCRIPT/Raster3D [14,15] stereodiagram and although the mean Cα deviations obtained were about 1 Å (1.06 Å for the superimposition c_3 and 9Hcc-N; 0.82 Å for the superimposition c_3 and 9Hcc-C) they nonetheless indicate a significant structural similarity between the compared regions, allowing the conclusion that the N-terminal and C-terminal domains in 9Hcc have a local fold that is similar to that of tetrahaem cytochrome c_3. The only substantial differences are due to the insertions associated with the isolated haem 4. The N-terminal domain of 9Hcc contains a tetrahaem c_3-like region and an insertion containing the binding region to haem 4, between the third (haem 3) and the fourth (haem 5) haem groups of the tetrahaem cluster, corresponding to a loop extension between the third and the fourth haem in the typical cytochrome c_3 fold. The C-terminal domain of 9Hcc, also with a tetrahaem c_3-like region has one insertion that contains the second histidine ligand of haem 4, instead of a short loop just before the first haem-binding region in *Dd* 27774 c_3. These domains are connected by a polypeptide segment 34 residues long, which may possibly act as a hinge, allowing the two tetrahaem c_3-like domains to move relative to each other. The domain structure in 9Hcc is shown as a MOLSCRIPT/Raster3D [14,15] stereo diagram in Figure 4. One important similarity can be found in the amino acid sequence motif P-X-X-F-X-H-X-X-H (Pro32–His40 and Pro192–His200 in 9Hcc) that also seems to exist in all the presently sequenced c_3 cytochromes from sulphate-reducing bacteria [6]. Another clear structural similarity is the presence of the motif C-X-X-C-H-H, which is also found in all known sequences of tetrahaem c_3 cytochromes, where the two cysteine residues bind the first haem group to the polypeptide chain, the first histidine is the first axial ligand of that haem group and the second histidine is the second axial ligand of the second haem group. In contrast, whereas in tetrahaem cytochrome c_3 from *Dd* 27774 the haem-binding regions of haem groups 2 and 4 are of the form C-X-X-X-X-C-H, in 9Hcc the haem-binding regions are all of the form C-X-X-C-H. The three-dimensional structures of two ditetrahaem cytochromes c_3, also referred to as cytochromes c_3 (Mr 26,000), from *Desulfomicrobium norvegicum* (previously known as *Desulfomicrobium baculatus* Norway 4) and *Desulfovibrio gigas* (*Dg*) have been determined [16,17]

Figure 4

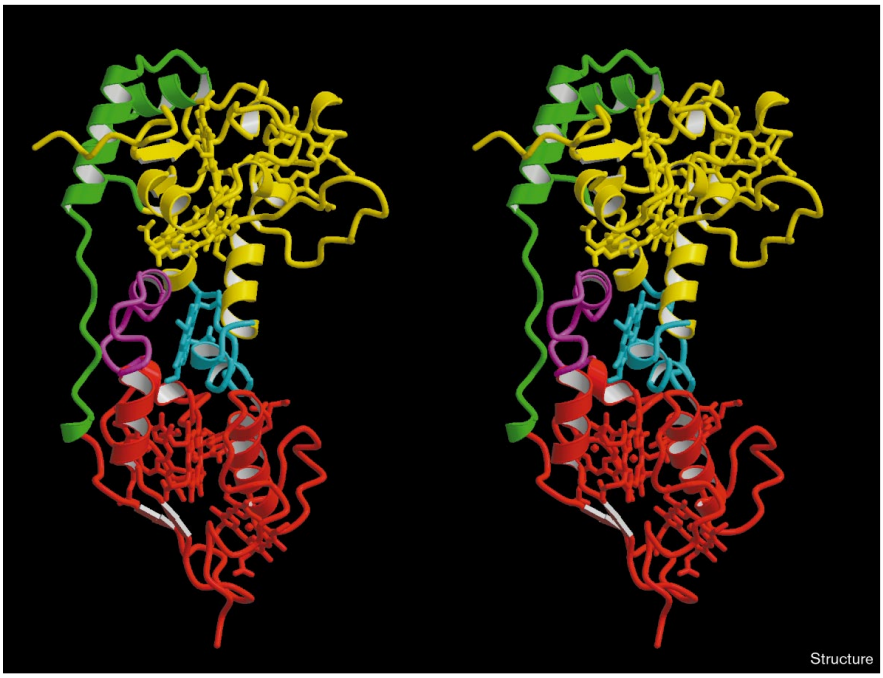

Domain structure of 9Hcc from *D. desulfuricans* ATCC 27774, established on the basis of comparison with the known structure of the tetrahaem cytochrome c_3 from the same organism. The different domains of the structure are colour-coded: the c_3-like tetrahaem region of the N-terminal domain is represented in yellow (residues 1–107 and 125–132); the insertion containing the isolated haem-binding region is drawn in cyan (residues 108–124); the polypeptide segment connecting the two domains is represented in green (residues 133–176); the c_3-like tetrahaem region of the C-terminal domain is in red (residues 177–205 and 224–292); and the insertion containing the second axial ligand of the isolated haem is shown in purple (residues 206–223).

and both have been found to be dimers of tetrahaem proteins, with a fold similar to, but amino acid sequence different from, the tetrahaem cytochromes c_3 also found in these organisms. The structure of the trimeric 24-haem enzyme hydroxylamine oxidoreductase has also been recently reported [18]; however, the folding and haem arrangement in this molecule bears no resemblance to the structures of either the tetrahaem c_3 cytochromes or 9Hcc. This is, therefore, the first known three-dimensional structure of a cytochrome in which multiple copies of a tetrahaem c_3-like fold are present in the same polypeptide chain.

Comparison with the high molecular weight cytochrome from *D. vulgaris* Hildenborough

A high molecular weight cytochrome (Hmc) containing the unprecedented number of 16 haem groups per molecule has been isolated from *Dv*H [19,20] and *D. vulgaris* Miyazaki (*Dv*M) [21] and also from *Dg* [22]. Cloning of the Hmc gene in *Dv*H revealed that it is part of a large operon encoding what seems to be a transmembrane redox complex, proposed to constitute the missing link between periplasmic hydrogen oxidation and cytoplasmic sulphate reduction [23], a central aspect of the *Desulfovibrio* metabolism. Although Hmc is not a hydrophobic protein, it can be isolated in larger amounts from membranes than from the soluble fraction, suggesting that it is attached to the membrane through the other proteins of the transmembrane redox complex [24]. Based on a sequence comparison of the haem-binding sites and second axial histidine ligands between the *Dv*H tetrahaem cytochrome c_3 and *Dv*H Hmc, it was proposed that *Dv*H Hmc is formed by four tetrahaem cytochrome c_3-like domains, the first one being an incomplete domain with only three haems [20]. As discussed in [22], this first domain is similar to the trihaem cytochrome c_3 from *Desulfuromonas acetoxidans*. Haem 12 of *Dv*H Hmc was proposed to be an isolated haem without bis-histidinyl coordination [20], located between the third and fourth domains, and so to be the high-spin haem in Hmc. The known amino acid sequence of *Dv*H Hmc [20] was aligned with that of 9Hcc as determined from the X-ray data. The first alignment was done by inspection, where all haem-binding motifs were tentatively superimposed, and the characteristic C-X-X-C-H-H motif was used as a reference point for the start of the possible tetrahaem c_3-like regions in both 9Hcc and Hmc. This first alignment gave a reasonable match between 9Hcc and the C-terminal region of Hmc (residues 229–514), and was refined by using CLUSTALW [25]. These results are shown in Figure 1 and show a significant degree of sequence homology, not only in terms of amino acid identity (113 out of 292, i.e. 38.7%) and similarity (a further 52, i.e. 17.8%; not included in Figure 1) but also in terms of the number of residues between each haem-binding motif. It is a well-known fact that tetrahaem cytochromes c_3 from sulphate-reducing bacteria have very similar three-dimensional structures in spite of occasional low sequence homologies [26–28]. Furthermore, with the exception of an eight-residue insertion that occurs in an exposed loop, all insertions and deletions in 9Hcc with respect to Hmc are only one or two residues long, and are thus not very likely to introduce large distortions in the

Figure 5

Stereoview figure illustrating the location of the insertions (red) and deletions (green) in *Dd* 27774 9Hcc with respect to the C-terminal region of *Dv*H Hmc. Deletions are defined by the adjacent two residues in *Dd* 27774 9Hcc. Single residue insertions are represented by red spheres at the Cα position of the inserted residue. The rest of the molecule is represented in light grey. The figure was made with the programs MOLSCRIPT/Raster3D [14,15].

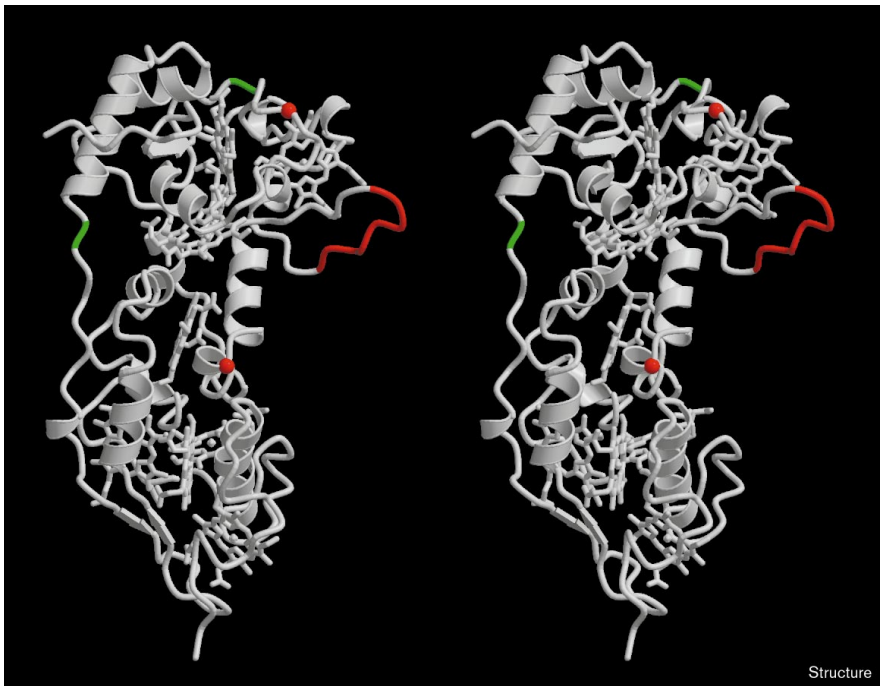

structure. Figure 5 shows the location of these insertions and deletions in the three-dimensional structure of 9Hcc. The first deletion is two residues long and occurs in the extended loop region between the first and the second strands of the initial two-stranded antiparallel β sheet found in all known three-dimensional structures of tetrahaem cytochromes c_3. Next, a one-residue insertion occurs in a short loop region between the haem-binding regions for haem groups 1 and 2 (presumably 8 and 9 in Hmc). Then, an eight-residue insertion occurs within an extended loop region that breaks up an α helix located between the haem-binding sites for haems 2 and 3 (9 and 10 in Hmc). A one-residue insertion is located in the middle of an α helix located between the haem attachment points for haem groups 3 and 4 (10 and 11 in Hmc), and appears to introduce a kink, causing this helix to break up into two shorter helical segments. Finally, a one-residue deletion occurs in 9Hcc at the C-terminal end of an α helix that is located in the segment of polypeptide chain connecting the N-terminal and C-terminal domains in 9Hcc. After this, there are no further insertions or deletions. On the basis of the sequence homology found between 9Hcc and the C-terminal 285 residues of *Dv*H Hmc, and also on the fact that no Hmc was ever found in *Dd* 27774, we therefore propose the inclusion of 9Hcc in the Hmc family. Consequently, this work can be said to describe the first known three-dimensional structure of an Hmc protein and provides a glimpse, albeit incomplete, into the three-dimensional structures of the Hmc molecules from *Desulfovibrio* organisms, in particular that of *Dv*H.

The sequence comparison between *Dd* 27774 9Hcc and *Dv*H Hmc also reveals that the proposed haem arrangement of domains III and IV of *Dv*H Hmc [20] is probably incorrect. If the haem-binding sites and second axial histidine ligands of *Dv*H Hmc are assigned according to the structure of 9Hcc (see Table 2) it can be seen that His439 of Hmc will most likely bind to haem 11 and not to haem 15 as previously proposed [20], and also that His310 will bind to haem 12 and not to haem 11 as previously proposed [20]. As a consequence, the high-spin haem of Hmc is not haem 12, but most likely haem 15, which corresponds to haem 8 of 9Hcc. This haem is bound by His200 in 9Hcc, which is replaced by Ile421 in *Dv*H Hmc. Since

Table 2

Alignment of haem number and respective second axial histidine ligand between *Dd* 27774 9Hcc and *Dv*H Hmc.

Haem number in *Dd* 27774 9Hcc	Haem number in *Dv*H Hmc	Sixth ligand in *Dd* 27774 9Hcc	Sixth ligand in *Dv*H Hmc
1	8	His37	His267
2	9	His52	His282
3	10	His40	His270
4	11	His218	His439
5	12	His81	His310
6	13	His197	His418
7	14	His230	His451
8	15	His200	–
9	16	His264	His485

Figure 6

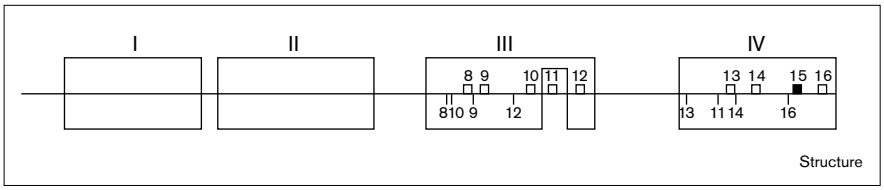

Schematic representation of the proposed structure for *Dv*H Hmc domains III and IV (adapted from [20]) based on the structure of *Dd* 27774 9Hcc. The squares represent haem-binding sites and the lines below the second axial histidine ligands. The haem-binding sites are numbered according to their position in the polypeptide from the N to the C terminus, and the numbers of the histidines correspond to the haem to which they are proposed to bind. The third cytochrome c_3-like domain is formed by haems 8, 9, 10 and 12, whereas haem 11 is an isolated haem. Haem 15 (filled square) is a high-spin haem with no second axial ligand. The haem-binding sites of the first and second domain are not shown as there are no proposed changes therein.

His200 is located towards the middle of an α helix (and presumably also Ile421), it is highly unlikely that the second axial ligand position of haem 15 of Hmc will be occupied by another residue.

Another interesting feature in the structure of these two cytochromes is the presence of an isolated haem group, not associated with a cytochrome c_3-like region. On the basis of sequence comparison with tetrahaem cytochrome c_3, the isolated haem of Hmc was proposed to be haem 12 [20]. However, the three-dimensional structure of 9Hcc reveals that the isolated haem of Hmc should in fact be haem 11, intercalated between the third and fourth haem groups of Hmc domain III (c_3-like region of the N-terminal domain in 9Hcc). In conclusion, the structure of *Dd* 27774 9Hcc and its sequence similarity to *Dv*H Hmc leads us to propose a different structural arrangement for haem domains III and IV of Hmc. In terms of the domain structure previously presented [20], we propose that in *Dv*H Hmc, His439 binds to haem 11, that His310 binds to haem 12, that haem 11 is an isolated haem outside the cytochrome c_3-like domains and that haem 15 is the high-spin haem of Hmc. This means that Hmc domain III will be formed by haems 8, 9, 10 and 12 and that the high-spin haem is the third haem in Hmc domain IV. Using the same type of schematic representation as before [20], the proposed structure of *Dv*H Hmc domains III and IV is shown in Figure 6. As clearly shown by our previous discussion concerning the domain structure of 9Hcc, however, domains III and IV of Hmc cannot be regarded further in terms of three-dimensional structure as pure tetrahaem cytochrome c_3-like domains. Instead, these domains can be thought of as c_3-like regions within more complex domains, which must also include the insertion regions binding haem 11.

Physiological role

It has recently been found that the *Dv*H Hmc is a very poor direct electron acceptor of either the [NiFe] or [Fe] hydrogenases, but that when cytochrome c_3 is present in catalytic amounts its reduction proceeds much more efficiently [29]. This means that physiologically, Hmc will most probably receive electrons from either hydrogenase via cytochrome c_3, transferring them afterwards to the transmembrane redox complex which will in turn donate them for the cytoplasmic reduction of sulphate. Hmc has never been found in *Dd* 27774 (J Le Gall *et al.*, unpublished results), and given the similarity between 9Hcc and *Dv*H Hmc, we believe that 9Hcc may be the equivalent of Hmc in *Dd* 27774. For this reason, the reaction of 9Hcc with [NiFe] hydrogenase from *Dd* 27774 (the only hydrogenase known in *Dd* 27774) was studied, both in the presence and in the absence of *Dd* 27774 tetrahaem cytochrome c_3. We observed that 9Hcc could be reduced directly by hydrogenase with a reasonable rate (4 nmolCyt.min^{-1}.nmolH_2ase^{-1}), but that in the presence of cytochrome c_3 this rate is considerably increased (20 nmolCyt.min^{-1}. nmolH_2ase^{-1}). This suggests that *in vivo*, and by analogy with Hmc, 9Hcc will most probably receive electrons from hydrogenase via cytochrome c_3, both of which are present in the cell in much higher amounts than 9Hcc. It is possible that the 9Hcc will also be associated with a transmembrane redox complex through which electrons are transferred to the cytoplasm for the reduction of sulphate. Another possibility is that 9Hcc itself might span the cytoplasmic membrane (between 60 and 100 Å wide), given its elongated rather than globular shape, with a longest dimension of about 77 Å. Such an arrangement could provide an explanation for the rather puzzling results, based on modelling studies, that the tetrahaem cytochrome c_3, which is located in the periplasm, can form specific complexes with redox partners such as ferredoxin [30], flavodoxin [31–33] and rubredoxin [34] which are found in the bacterial cytoplasm. These separate locations make the physiological significance of such interactions quite doubtful; however, as both ends of 9Hcc are structurally similar to the tetrahaem cytochrome c_3, one end could be specialised for interaction with the periplasmic proteins whereas the other would react more specifically with the cytoplasmic redox carriers. Experiments aimed at testing this hypothesis are underway in our laboratories.

Biological implications

Sulphate-reducing bacteria grow by the anaerobic respiration of sulphate, which is reduced to sulphide. Contrary

to most other bacteria, the terminal reductases involved in the reduction of sulphate are not membrane-bound but cytoplasmic, and so cannot be directly associated with proton translocation across the membrane. The fundamental question of how these bacteria achieve energy conservation is still not fully understood, but will most likely involve a membrane-bound electron transport chain. Bacteria of the *Desulfovibrio* genus, the best studied genus of the sulphate reducers, are characterised by having one or more hydrogenases and large amounts of a periplasmic tetrahaem cytochrome c_3 that seem to play a central role in the metabolism. In particular, several of these organisms are capable of growing using hydrogen as the only electron donor. This hydrogen is oxidised by a hydrogenase in the periplasm, which will donate electrons to cytochrome c_3. In *Desulfovibrio vulgaris* Hildenborough (*Dv*H) it was proposed that this reducing power was transferred from cytochrome c_3 via the 16-haem high molecular weight cytochrome (Hmc) and its associated transmembrane redox complex [29] to the terminal reductases responsible for the cytoplasmic reduction of sulphate. Growth studies with wild-type and mutant strains of *Dv*H showed that Hmc and its complex are indeed strongly implicated in the metabolism of hydrogen [35]. In *Desulfovibrio desulfuricans* (*Dd*) 27774, a 16-haem Hmc could not be found. Given the strong sequence similarity between *Dv*H Hmc and *Dd* 27774 nine-haem cytochrome *c* (9Hcc), and their similar behaviour with respect to reduction by hydrogenase, we propose that 9Hcc replaces Hmc in *Dd* 27774, that it acts as an electron acceptor for cytochrome c_3 and that it is involved in electron transfer across the membrane. As such, we propose that 9Hcc be considered as a member of the Hmc family.

Materials and methods

Crystallisation

Crystals of 9Hcc were obtained by the sitting drop vapour diffusion method as previously described [6]. The crystals belong to monoclinic space group $P2_1$, room temperature cell parameters $a = 61.00$ Å, $b = 106.19$ Å, $c = 82.05$ Å, $\beta = 103.61°$. The MAD [8] method, using the Fe atoms in the native protein as anomalous scatterers, was used for the determination of the three-dimensional structure of this protein. All data were measured from the same flash frozen crystal in order to withstand the radiation damage caused by prolonged exposure to synchrotron X-rays. The best cryocrystallography conditions for this protein were obtained by preparing a solution with the same composition as above, plus 20% glycerol. The best results for flash freezing crystals of 9Hcc were obtained when the crystals were dipped only briefly (~30 seconds) in the cryoprotecting solution. In this fashion, the mosaicity of the crystals did not increase significantly when compared with typical values (0.3–0.4°) at room temperature.

Data collection and processing

Synchrotron diffraction data were collected using a MAR Research 345 imaging plate system (in 300 mm scanning mode with 150 μm pixel size) at ESRF BM14, from a frozen crystal of 9Hcc (dimensions $0.2 \times 0.2 \times 0.1$ mm^3) at three suitable wavelengths near the Fe absorption edge, chosen from an X-ray fluorescence scan of a frozen crystal. This scan showed an extra XANES feature at the absorption edge making the identification of the f′ minimum difficult, therefore the following wavelengths were selected: λ_1 1.7377 Å, to maximise $\Delta f''$ (peak), λ_2 1.7398 Å, at the first point of inflexion and λ_3, 1.7408 Å, at the second point of inflexion. A fourth wavelength, λ_4 0.8856 Å, was used as the reference wavelength, to facilitate scaling of the data by minimising absorption problems which might be present at the other three wavelengths. The unit cell parameters at 105K were $a = 60.48$ Å, $b = 106.33$ Å, $c = 80.80$ Å, $\beta = 103.51°$. The diffraction images were processed and scaled with the HKL suite [36]. The scaling was carried out in such a way as to preserve the multiple observations of all the measured Bijvoet mates. The CCP4 [37] program suite was then used to merge together the scaled data (ROTAPREP/AGROVATA), convert intensities to structure factors (TRUNCATE, [38]) and to scale together the different wavelength data relatively to λ_4 (SCALEIT). The data collection, processing and scaling statistics are summarised in Table 3. The λ_4 data were recorded in two passes. In the first pass, data were collected to 1.8 Å resolution, and in the second pass a data set to 2.9 Å resolution was measured, in order to fill in the low resolution reflections missing from the first pass due to detector saturation. Each of these passes was processed and scaled as a separate data set as described above. Each was assigned a different batch number and the ROTAPREP results were first combined with SORTMTZ and then scaled together with ROTAVATA prior to merging with AGROVATA and conversion of intensities to structure factors with TRUNCATE.

Structure determination and model building

MADLSQ and MERGIT in the MADSYS [8] program suite were used to extract F^o_A values (i.e., the normal scattering component of the anomalously scattering atoms) from the scaled data. Normalised F^o_A amplitude values obtained with ECALC (CCP4) were used to calculate an origin-removed Patterson map. SHELXS-96 [39] was used to locate all 18 Fe sites (nine per molecule) from the F^o_A values ($2.9 \leq d \leq 15$ Å) by means of a Patterson superposition vector search method combined with partial structure expansion via a direct method approach. The Fe atom positions were refined and used to derive phase information with MLPHARE [40] following the pseudo-MIR procedure as previously described (e.g., see [41–43]). Phase refinement with MLPHARE in the resolution range $10 \geq d \geq 2.9$ Å converged to an overall figure of merit of 0.775. A summary of the phase refinement statistics is included in Table 3. The refined Fe atomic positions were used to derive the noncrystallographic symmetry (NCS) operation between the two independent molecules (LSQKAB [44] and IMP [45]) which was found to be consistent with the self-rotation function results previously reported [6].

Density modification procedures (DM) [46], which included averaging, solvent flattening, histogram matching and phase extension ($20 \geq d \geq 2.4$ Å) using the structure factors from the remote (λ_4) dataset, produced a much improved electron-density map over that obtained from the original MAD phases. This map was of excellent quality and allowed a complete trace of the electron density. The initial model was built with O [47] (chain trace, backbone building) and TURBO [13] (sidechain rotamer selection) and contained 289 residues and nine haem groups. A perfect fit of the electron density to the known 39 N-terminal amino acids [6] was observed, except for Ala1, which was not visible, and Glu21 and Lys22, for which no sidechain electron density was visible, and most of the remaining sidechains were then assigned by inspection.

Refinement

Model refinement began with X-PLOR [48] with the remote data set to 2.4 Å, using mainchain and sidechain NCS restraints between the two independent molecules in the asymmetric unit. Initial values of R and R_{free} [49] (based on a random sample of 5% of the reflections in the remote dataset) were 37.6% and 38.7%, respectively. The standard X-PLOR simulated annealing protocol at 3000K was used and, following convergence, the same protocol was applied to the full 1.8 Å remote data set, first with NCS restraints and then a second time without restraints, leading to R and R_{free} values of 25.5% and 28.1% respectively, after refinement of individual restrained B factors. Several 1000K annealed omit maps were calculated to verify and correct the

Table 3

Data collection, processing, scaling and phase refinement statistics.

Wavelength	λ_1 (1.7377 Å)	λ_2 (1.7398 Å)	λ_3 (1.7408 Å)	λ_4 (0.8856 Å)
d_{min} (Å)	24.9	25.0	24.9	24.2
d_{max} (Å)	2.90	2.90	2.90	1.80
No. observations	83,071	82,978	82,971	425,233
No. reflections	21,987	22,041	21,915	91,192
Completeness (%)	99.4 (97.0)	99.6 (98.6)	99.0 (93.3)	98.8 (93.1)
Multiplicity	3.8 (3.7)	3.8 (3.7)	3.8 (3.7)	4.7 (3.7)
$R_{merge}(I)$	0.042 (0.065)	0.041 (0.065)	0.042 (0.068)	0.034 (0.116)
$R_{anom}(I)$	0.063 (0.081)	0.050 (0.066)	0.037 (0.052)	0.025 (0.077)
No. Bijvoet pairs	17,150	17,170	17,046	75,673
Bijvoet completeness (%)	81.2	81.1	81.0	85.1
$I/\sigma(I)$	14.1 (9.7)	14.3 (9.7)	13.8 (9.2)	16.8 (6.2)
Scaling R factor (F)	0.056	0.072	0.066	–
Phasing power				
acentric	1.57	–	0.58	3.34
centric	1.19	–	0.38	2.78
R_{cullis}				
acentric	0.68	–	0.94	0.41
centric	0.62	–	0.94	0.34
anomalous	0.43	0.49	0.72	0.77

Values in parentheses refer to the last resolution shell: $3.06 \geq d \geq 2.90$ Å for λ_1, λ_2 and λ_3, $1.87 \geq d \geq 1.80$ Å for λ_4. The multiplicity values are overall values, that is, no distinction is made between Bijvoet pairs. The percentage of Bijvoet completeness is calculated as the ratio between the number of pairs recorded and the total number of acentric reflections measured. Scaling R factor (F) $= \sum_{hkl} |F_{\lambda i} - F_{\lambda 4}| / \sum_{hkl} F_{\lambda 4}$.

sidechain assignments made, and a total of 750 solvent molecules and five acetate ions were included in the model. The criteria for including water molecules were that they should be visible as peaks higher than 3 rms in the $|F_o|-|F_c|$ electron-density map, as peaks higher than 1 rms in the $2|F_o|-|F_c|$ map, and should have distances to suitable donors or acceptors of hydrogen bonds between 2.4 and 3.2 Å. Also, the number of residues was extended to 292, Ala1 being included in the N-terminal region and two other alanine residues in the C-terminal region. The refinement results with X-PLOR gave R and R_{free} values of 18.5% and 21.4%, respectively. The final refinements were carried out on F_o^2 with SHELXL [50], first using a test set for R_{free} calculation identical to that used in X-PLOR, and upon convergence (R = 17.8%, R_{free} = 21.9%) using all 91,192 independent reflections. A further 136 solvent molecules were included in the model, applying the criteria outlined above. In addition, the occupation factors of all solvent oxygen atoms whose isotropic thermal motion parameter became higher than 50 Å^2 were arbitrarily set to 1/2. Anisotropic thermal motion parameters were refined for all the Fe and S atoms in the model, and an overall anisotropic scaling procedure between F_o and F_c was used. This refinement converged to R = 17.0%. The final model includes some twofold disordered regions: Ser58 (0.66), Ile74 (0.54), Gln102–Ser103 (0.69), Val172 (0.51), Glu206 (0.61) and Ser243 (0.57) in molecule A; Ile117–Pro120 (0.53), Glu191 (0.55) and Glu206 (0.63) in molecule B (values in parentheses represent the refined occupation factor of the major component). Of the 292 residues in the model, only 8 (i.e., 3% of the unknown 253 residues) remain to be identified, apart from ambiguities between Asp/Asn and Glu/Gln residues, particularly those located on the surface of the molecule, which cannot be resolved at 1.8 Å resolution. The final refinement statistics are presented in Table 4. The model was analysed with PROCHECK [9] and both molecules had stereochemical quality parameters within their respective confidence intervals. In the ψ,ϕ plots for the non-proline and non-glycine residues (not shown) only Asp188 lies slightly outside the normally allowed regions. Overall, 86.9% of the residues in molecule A and 88.1% of the residues in molecule B lie within the most favoured regions. The φ,ϕ plots for proline and glycine residues (not shown) indicate that none of these residues adopts any unusual ψ,ϕ conformations. Both molecules were assigned a G factor of 0.0 and to (1 1 2) classes as defined by Morris *et al.* [51]. In both molecules, Pro279 has a *cis*-peptide bond.

Table 4

Final refinement statistics for 9Hcc.

Resolution limits (Å)	24.0–1.80
Final R factor (%) (all 91,192 reflections)	17.0
No. nonhydrogen protein atoms*	5,109
No. nonhydrogen protein atoms in disordered residues†	77
No acetate ions/atoms	5/20
No. solvent molecules with full occupancy	709
No. solvent molecules with 1/2 occupancy	173
No. solvent molecules with disorder	4
No. least-squares parameters	24,762
No. restraints in final least-squares cycle	24,527
Disagreeable restraints ($\Delta > 3\sigma$)‡	
FLAT	6
SIMU	7
Estimated overall rms coordinate error (Å)§	0.04
Model rms deviations from ideality#¶¥	
bond lengths (Å) (A/B)	0.02/0.02
bond angles (°) (A/B)	2.19/2.15
Average B values (Å^2)¶¥	
mainchain protein (A/B)	17.7/20.9
sidechain protein (A/B)	20.7/23.8
haem groups (A/B)	14.0/18.2
solvent (including acetate ions)	29.7

*Excluding atoms in the minor component of disordered regions. †Atoms in the minor disorder component. ‡Restraints defined according to SHELXL convention [50]. §Calculated with SIGMAA [37,54]. #Calculations performed with X-PLOR using the final SHELXL model. ¶For the disordered residues, only the major component atoms were considered. ¥A/B refer to the two molecules in the asymmetric unit.

Kinetic reduction experiments

The reduction experiments of 9Hcc by the *Dd* 27774 [NiFe] hydrogenase were performed as described in [29] using the following concentrations: 9Hcc, 1 μM; *Dd* 27774 [NiFe] hydrogenase, 110 nM; *Dd* 27774 cytochrome c_3, 110 nM.

Accession numbers

The coordinates of the refined 9Hcc model have been deposited in the Protein Data Bank [52,53] with accession code 1c9h.

Acknowledgements

This work was funded by European Union (Network CHRX-CT93-0143 and grant BI02/CT94/2052) and JNICT (grants PMCT/C/BIO/874/90 and PRAXIS/2/2.1/QUI/17/94). The authors would like to thank the fermentation plant at University of Georgia, Athens, GA, USA for growing the bacteria, M-Y Liu (UGA) and Isabel Pacheco (ITQB-UNL) for the purified protein samples used for crystallisation, António V Xavier (ITQB-UNL) for stimulating discussions and valuable suggestions in the course of this work, David Marçal and Sofia Macedo (ITQB-UNL) for help with the crystallisation experiments and ESRF for support for the BM14 data collection.

References

1. Pereira, I.A.C., Teixeira, M. & Xavier, A.V. (1998). Hemeproteins in anaerobes. *Structure Bonding* **91**, 65-89.
2. Yagi, T., Honya, M. & Tamiya, N. (1968). Properties of hydrogenase of different origins. *Biochem. Biophys. Acta* **153**, 699-705.
3. Louro, R.O., Catarino, T., Salgueiro, C.A., Le Gall, J. & Xavier, A.V. (1996). Redox-Bohr effect in the tetrahaem cytochrome c_3 from *Desulfovibrio vulgaris*: a model for energy transduction mechanisms. *J. Biol. Inorg. Chem.* **1**, 34-48.
4. Louro, R.O., Catarino, T., Le Gall, J. & Xavier, A.V. (1997). Redox-Bohr effect in electron/proton energy transduction: cytochrome c_3 coupled to hydrogenase works as a "proton thruster" in *Desulfovibrio vulgaris*. *J. Biol. Inorg. Chem.* **2**, 488-491.
5. Liu, M.-C., *et al*., & Le Gall, J. (1988). Cytochrome components of nitrate- and sulfate-respiring *Desulfovibrio desulfuricans* ATCC 27774. *J. Bacteriol.* **170**, 5545-5551.
6. Coelho, A.V., *et al*., & Le Gall, J. (1996). Preliminary crystallographic analysis and further characterization of a dodecaheme cytochrome *c* from *Desulfovibrio desulfuricans* ATCC 27774. *Acta Crystallogr. D* **52**, 1202-1209.
7. Fuhrhop, J.-H. & Smith, K.M. (1975). Laboratory methods. In *Porphyrins and Metalloporphyrins.* (Smith, K.M., ed.), pp. 757-861, Elsevier Press, Amsterdam, The Netherlands.
8. Hendrickson, W.A. (1991). Determination of macromolecular structures from anomalous diffraction of synchrotron radiation. *Science* **254**, 51-58.
9. Laskowski, R.A., MacArthur, M.W., Moss, D.S. & Thornton, J.M. (1993). PROCHECK – a program to check the stereochemical quality of proteins. *J. Appl. Crystallogr.* **26**, 283-291.
10. Kabsch, W. & Sander, C. (1983). Dictionary of protein secondary structure: pattern recognition of hydrogen-bonded and geometrical features. *Biopolymers* **22**, 2577-2637.
11. Simões, P., Matias, P.M., Morais, J., Wilson, K., Dauter, Z. & Carrondo, M.A. (1998). Refinement of the three-dimensional structures of cytochrome c_3 from *Desulfovibrio vulgaris* Hildenborough at 1.67 Å resolution and from *Desulfovibrio desulfuricans* ATCC 27774 at 1.6 Å resolution. *Inorg. Chim. Acta* **273**, 213-224.
12. Lee, B., Richards, F.M. (1971). The interpretation of protein structures: estimation of static accessibility. *J. Mol. Biol.* **55**, 379-400.
13. Roussel, A., Fontecilla-Camps, J.C., Cambillau, C. (1990). TURBO-FRODO: a new program for protein crystallography and modelling. XV IUCr Congress Abstracts, Bordeaux, France, pp. 66-67.
14. Kraulis, P.J. (1991). MOLSCRIPT: a program to produce both detailed and schematic plots of protein structures. *J. Appl. Crystallogr.* **24**, 946-950.
15. Merritt, E.A. & Murphy, M.E.P. (1994). Raster3D version 2.0. A program for photorealistic molecular graphics. *Acta Crystallogr. D* **50**, 869-873.
16. Czjzek, M., Guerlesquin, F., Bruschi, M. & Haser, R. (1996). Crystal structure of a dimeric octaheme cytochrome c_3 (M_r 26 000) from *Desulfovibrio desulfuricans* Norway. *Structure* **4**, 395-404.
17. Frazão, C., Sieker, L., Sheldrick, G., Lamzin, V., LeGall J. & Carrondo, M.A. (1998). *Ab initio* structure solution of a dimeric cytochrome c_3 from *Desulfovibrio gigas* containing disulphide bridges. *J. Biol. Inorg. Chem.*, in press.
18. Igarashi, N., Moriyama, H., Fujiwara, T., Fukumori, Y. & Tanaka, N. (1997). The 2.8 Å structure of hydroxylamine oxidoreductase from a nitrifying chemoautotrophic bacterium, *Nitrosomas europaea*. *Nat. Struct. Biol.* **4**, 276-284.
19. Higuchi, Y., Inaka, K., Yasuoka, N. & Yagi, T. (1987). Isolation and crystallization of high molecular weight cytochrome from *Desulfovibrio vulgaris* Hildenborough. *Biochem. Biophys. Acta* **911**, 341-348.
20. Pollock, W.B.R., *et al*., & Voordouw, G. (1991). Cloning, sequencing and expression of the gene encoding the high-molecular-weight cytochrome *c* from *Desulfovibrio vulgaris* Hildenborough. *J. Bacteriol.* **173**, 220-228.
21. Ogata, M., Kiuchi, N. & Yagi, T. (1993). Characterization and redox properties of high molecular mass cytochrome c_3 (Hmc) isolated from *Desulfovibrio vulgaris* Miyazaki. *Biochimie* **75**, 977-983.
22. Chen, L., Pereira, M.M., Teixeira, M., Xavier, A.V. & Le Gall, J. (1994). Isolation and characterization of a high molecular weight cytochrome from the sulfate reducing bacterium *Desulfovibrio gigas*. *FEBS Lett.* **347**, 295-299.
23. Rossi, M., Pollock, W.B.R., Reij, M.W., Keon, R.G., Fu, R. & Voordouw, G. (1993). The *hmc* operon of *Desulfovibrio vulgaris* subsp. *vulgaris* Hildenborough encodes a potential transmembrane redox protein complex. *J. Bacteriol.* **175**, 4699-4711.
24. Pereira, I.A.C., Le Gall, J., Xavier, A.V. & Teixeira, M. (1997). The membrane-bound high molecular weight cytochromes *c* from *Desulfovibrio gigas* and *Desulfovibrio vulgaris* Hildenborough: EPR and Mössbauer studies. *J. Biol. Inorg. Chem.* **2**, 23-31.
25. Thompson, J.D., Higgins, D.G. & Gibson, T.J. (1994). CLUSTAL W: improving the sensitivity of progressive multiple sequence alignment through sequence weighting, positions-specific gap penalties and weight matrix choice. *Nucleic Acids Res.* **22**, 4673-4680.
26. Matias, P.M., Frazão, C., Morais, J., Coll, M. & Carrondo, M.A. (1993). Structure analysis of cytochrome c_3 from *Desulfovibrio vulgaris* Hildenborough at 1.9 Å resolution. *J. Mol. Biol.* **234**, 680-699.
27. Czjzek, M., Payan, F., Guerlesquin, F., Bruschi, M. & Haser, R. (1994). Crystal structure of cytochrome c_3 from *Desulfovibrio desulfuricans* Norway at 1.7 Å resolution. *J. Mol. Biol.* **243**, 653-667.
28. Matias, P.M., *et al*., & Sieker, L. (1996). Cytochrome c_3 from *Desulfovibrio gigas*: crystal structure at 1.8 Å resolution and evidence for a specific calcium-binding site. *Protein Sci.* **5**, 1342-1354.
29. Pereira, I.A.C., Romão, C.V., Xavier, A.V., Le Gall, J. & Teixeira, M. (1998). Electron transfer between hydrogenases and mono and multiheme cytochromes in *Desulfovibrio spp. J. Biol. Inorg. Chem.* **3**, 494-498.
30. Cambillau, C., Frey, M., Mosse, J., Guerlesquin, F. & Bruschi, M. (1988). Model of a complex between the tetrahemic cytochrome c_3 and the ferredoxin I from *Desulfovibrio desulfuricans* (Norway Strain). *Proteins* **4**, 63-70.
31. Stewart, D.E., *et al*., & Wampler, J.E. (1988). A hypothetical model of the flavodoxin-tetra heme cytochrome c_3 complex of sulfate reducing bacteria. *Biochemistry* **27**, 2444-2450.
32. Palma, P.N., Moura, I., Le Gall, J., Van Beeumen, J.E., Wampler, J.E. & Moura, J.J.G. (1994). Evidence for a ternary complex formed between flavodoxin and cytochrome c_3. ^{1}H NMR and molecular modeling studies. *Biochemistry* **33**, 6394-6407.
33. De Francesco, R., Edmonson, D.E., Moura, I., Moura, J.J.G. & Le Gall, J. (1994). Kinetic studies on the electron transfer reaction between cytochrome c_3 and flavodoxin from *Desulfovibrio vulgaris* strain Hildenborough. *Biochemistry* **33**, 10386-10392.
34. Stewart, D.E., *et al*., & Wampler, J.E. (1989). Electron transport in sulfate-reducing bacteria: molecular modeling and NMR studies of the rubredoxin-tetraheme cytochrome c_3 complex. *Eur. J. Biochem.* **185**, 695-700.
35. Keon, R.G., Fu, R. & Voordouw, G. (1997). Deletion of two downstream genes alters expression of the *hmc* operon of *Desulfovibrio vulgaris* subsp. *vulgaris* Hildenborough. *Arch. Microbiol.* **167**, 376-383.
36. Otwinowski, Z. & Minor, W. (1997). Processing of X-ray diffraction data collected in oscillation mode. In *Methods in Enzymology, Volume 276: Macromolecular Crystallography Part A.* (Carter, C.W., Jr. & Sweet, R.M., eds), pp. 307-326, Academic Press, New York, USA.
37. Collaborative Computational Project Number 4. (1994). The CCP4 suite: programs for protein crystallography. *Acta Crystallogr. D* **50**, 760-763.
38. French, G.S. & Wilson, K.S. (1978). On the treatment of negative intensity observations. *Acta. Crystallogr. A* **34**, 517-525.
39. Sheldrick, G.M. (1997). Patterson superposition and *ab initio* phasing. In *Methods in Enzymology, Volume 276: Macromolecular Crystallography Part A.* (Carter, C.W., Jr. & Sweet, R.M., eds), pp. 628-641, Academic Press, New York, USA.

40. Otwinowski, Z. (1991). Isomorphous refinement and anomalous scattering. In *Proceedings of the CCP4 Study Weekend.* (Wolf, W., Evans, P.R. & Leslie, A.G.W., eds), pp. 80-86, SERC Daresbury Laboratory, UK.
41. Ramakrishnan, V., Finch, J.T., Graziano, V., Lee, P.L. & Sweet, R.M. (1993). Crystal structure of globular domain of histone H5 and its implications for nucleosome binding. *Nature* **362**, 219-223.
42. Glover, I., *et al*., & Tame, J.R.H. (1995). Structure determination of OppA at 2.3 Å resolution using multiple-wavelength anomalous dispersion methods. *Acta Crystallogr. D* **51**, 39-47.
43. Matias, P.M., *et.al*., & Carrondo, M.A. (1997). A preliminary analysis of the three-dimensional structure of dimeric di-heme split-Soret cytochrome *c* from *Desulfovibrio desulfuricans* ATCC 27774 at 2.5 Å resolution using the MAD phasing method: a novel cytochrome fold with a stacked heme arrangement. *J. Biol. Inorg. Chem.* **2**, 507-514.
44. Kabsch, W. (1976). A solution for the best rotation to relate two sets of vectors. *Acta. Crystallogr. A* **32**, 922-923.
45. Kleywegt G.J. & Read, R.J. (1997). Not your average density. *Structure* **5**, 1557-1569.
46. Cowtan, K. (1994). 'DM': an automated procedure for phase improvement by density modification. *Joint CCP4 and ESF-EACBM Newsletter on Protein Crystallography*. **31**, pp. 34-38.
47. Jones, T.A., Zou, J.Y., Cowan, S.W. & Kjeldgaard, M. (1991). Improved methods for building protein models in electron density maps and the location of errors in these models. *Acta Crystallogr. A* **47**, 110-119.
48. Brünger, A.T. (1992). X-PLOR, version 3.1: a system for X-ray crystallography and NMR. Yale University Press, New Haven CT, USA.
49. Brünger, A.T. (1992). Free R value: a novel statistical quantity for assessing the accuracy of crystal structures. *Nature* **355**, 472-474.
50. Sheldrick, G.M. & Schneider, T.R. (1997). SHELXL: high-resolution refinement. In *Methods in Enzymology, Volume 277: Macromolecular Crystallography Part B.* (Carter, C.W., Jr. & Sweet, R.M., eds), pp. 319-343. Academic Press, New York, USA.
51. Morris, A.L., MacArthur, M.W., Hutchinson, E.G. & Thornton, J.M. (1992). Stereochemical quality of protein structure coordinates. *Proteins* **12**, 345-364.
52. Abola, E.E., Bernstein, F.C., Bryant, S.H., Koetzle, T.F. & Weng, J. (1987). Protein Data Bank. In *Crystallographic Databases – Information Content, Software Systems, Scientific Applications*. (Allen, F.H., Bergeroff, G. & Sievers, R., eds), pp. 107-132, Data Commission of The International Union of Crystallography, Cambridge.
53. Bernstein, F.C., *et al*., & Tasumi, M. (1977). The Protein Data Bank: a computer-based archival file for macromolecular structures. *J. Mol. Biol.* **112**, 535-542.
54. Read, R.J. (1986). Improved Fourier coefficients for maps using phases from partial structures with errors. *Acta. Crystallogr. A* **42**, 140-149.